JACS JOURNAL OF THE AMERICAN CHEMICAL SOCIETY

Perspective

Cite This: J. Am. Chem. Soc. 2019, 141, 2179–2193

pubs.acs.org/JACS

Nanoscale Surface Structure–Activity in Electrochemistry and Electrocatalysis

Cameron L. Bentley,* Minkyung Kang, and Patrick R. Unwin*

Department of Chemistry, University of Warwick, Coventry CV4 7AL, U.K.

ABSTRACT: Nanostructured electrochemical interfaces (electrodes) are found in diverse applications ranging from electrocatalysis and energy storage to biomedical and environmental sensing. These functional materials, which possess compositional and structural heterogeneity over a wide range of length scales, are usually characterized by classical macroscopic or "bulk" electrochemical techniques that are not well-suited to analyzing the nonuniform fluxes that govern the electrochemical response at complex interfaces. In this Perspective, we highlight new directions to studying fundamental electrochemical and electrocatalytic phenomena, whereby nanoscale-resolved information on activity is related to electrode structure and properties colocated and at a commensurate scale by using complementary high-resolution microscopy techniques. This *correlative electrochemical multimicroscopy* strategy aims to unambiguously resolve structure and activity by identifying and characterizing the structural features that constitute an active surface, ultimately facilitating the rational design of functional electromaterials. The discussion encompasses high-resolution correlative structure–activity investigations at well-defined surfaces such as metal single crystals and layered materials, extended structurally/compositionally heterogeneous surfaces such as polycrystalline metals, and ensemble-type electrodes exemplified by nanoparticles on an electrode support surface. This Perspective provides a roadmap for next-generation studies in electrochemistry and electrocatalysis, advocating that complex electrode surfaces and interfaces be broken down and studied as a set of simpler "single entities" (e.g., steps, terraces, defects, crystal facets, grain boundaries, single particles), from which the resulting nanoscale understanding of reactivity can be used to create rational models, underpinned by theory and surface physics, that are self-consistent across broader length scales and time scales.

1. INTRODUCTION

The structure of electrode surfaces has long been considered to have a profound effect on electrode kinetics and reaction mechanisms. Understanding structure–activity–selectivity relationships for electrocatalysts has arguably never been more important than today, with electrochemistry finding renewed interest in areas from organic synthesis to sensor technologies and being at the heart of energy storage and conversion technologies,[1] which need to be improved considerably and quickly if we are to move to a world of decarbonized energy. High-resolution microscopy has provided unprecedented views of the complexity of electrode surfaces. However, despite this acknowledged complexity, electrochemical measurements rely mainly on rather old macroscopic techniques that provide activity averaged over a wide range of interacting surface sites, thereby obscuring the nature of key elementary processes. The aim of this Perspective is to highlight opportunities for fundamental electrochemistry and electrocatalysis studies, whereby electrode activity and dynamics (electrochemical fluxes) can be visualized at the nanoscale in the form of electrochemical "activity pictures" and "activity movies", and further, where these high spatiotemporal resolution electrochemical data can be correlated directly with the underlying electrode structure and properties (electronic, chemical), obtained by using complementary high-resolution microscopy techniques in the same region of an electrode. This new age of *correlative electrochemical multimicroscopy* promises a much improved understanding of structural controls in electrocatalysis and will greatly advance the knowledge of electrochemical processes and facilitate rational catalyst design.

To illustrate the power of these approaches, we discuss a range of contemporary topical processes at different classes of electrodes used in electrochemistry. At the simplest level, the electrochemical processes can be divided into two categories (Figure 1): outer-sphere redox processes, where there is little or no physical interaction between the redox species and electrode surface, and where questions relate to the influence of local electronic structure (density of states), solvent/electrolyte properties and double layer effects on electrochemical processes (Figure 1a), and inner-sphere or catalytic redox processes, where the bonding or adsorption of reactants, intermediates, and/or products to the electrode surface has a profound effect on the electrode reaction kinetics (Figure 1b).[2,3] Outer-sphere redox processes are fully described by a formal reduction potential ($E^{\circ\prime}$), standard rate constant (k^0), and charge-transfer coefficient (α), as defined in the classical Butler–Volmer formalism of electrode kinetics, whereas inner-sphere (catalytic) processes are often benchmarked by an overpotential (η), Tafel slope (semiquantitative indicator of charge-transfer kinetics and/or mechanisms for simple processes), and/or exchange current density (j_0, equal to the current density, j, at the equilibrium potential, which is a quantitative indicator of charge-transfer kinetics), as defined in the well-known Tafel equation.[1,3,4]

The traditional approach for exploring the role of surface structure and defects in electrocatalysis has been to make use of single crystals of long-range order, prepared with a particular surface orientation (Figure 2a). Macroscopic electrochemical

Received: September 11, 2018
Published: November 28, 2018

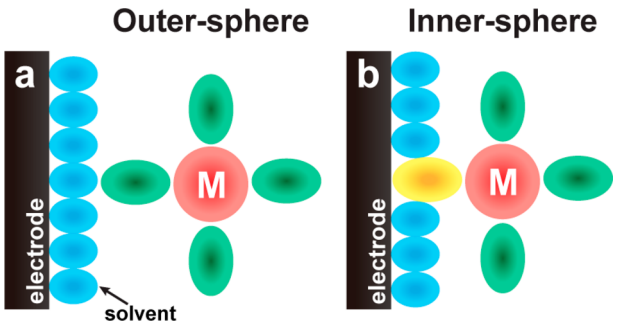

Figure 1. Mechanisms of heterogeneous electron transfer. (a) In an outer-sphere redox process, the reactant and product do not interact strongly with the electrode surface and electron transfer proceeds in the absence of bond breakage/formation. Examples considered herein include the $[Ru(NH_3)_6]^{2+/3+}$ and $[Fe(H_2O)_6]^{2+/3+}$ (in the absence of bridging ligands) processes in aqueous media. (b) In an inner-sphere (catalytic) redox process, reactants, intermediates, and/or products interact strongly with the electrode surface (specific adsorption) during the electrochemical process, which often involves the breakage or formation of chemical bonds. Examples considered herein include the $Fe^{2+/3+}$ process (in the presence of bridging ligands such as Cl^-), hydrogen evolution reaction, oxygen reduction reaction, and electrochemical CO_2 reduction.

measurements on such surfaces have been used to elucidate how structure influences activity, particularly for noble-metal electrodes.[5−7] However, single-crystal surfaces are not perfect over large areas, and even on the best-quality surfaces it is challenging to elucidate the roles of step edges and terraces.[8] As we discuss in section 2, high-resolution electrochemical measurements at characteristic individual "single-entity" surface sites are providing new perspectives on local activity at single-crystal surfaces and layered materials.

Electrodes of practical importance are often polycrystalline and, furthermore, may show compositional variations (Figure 2b). It is for this type of electrochemical interface that high-resolution correlative structure−activity investigations come into their own, by unambiguously and directly relating local electrochemical fluxes to the corresponding local surface structure (individual grains and grain boundaries (GBs)) and composition, as we discuss in section 3. Local electrochemical measurements are also powerful in detecting the transport of reactive intermediates between neighboring active sites on a surface and the synergistic operation of catalysts and electrocatalysts.[9,10] These aspects critical to the operation of electrocatalytic systems involving nanomaterials (e.g., nanoparticles, NPs) on electrode supports (Figure 2c) are completely hidden in macroscale measurements. A further consideration is the nanoscale diffusion and interaction of electrochemically generated reactive intermediates with the support, the possible (unwanted) products thereof, and, in turn, their interaction with the electrocatalyst. The physicochemical stability of the system (e.g., NP−substrate interactions, attachment, migration, dissolution−growth−ripening, etc.) during, and as a consequence of, the electrochemical process must be considered. These key issues have brought about a diversity of different approaches to assess NP activity and stability, the relative merits of which are assessed and discussed in section 4.

2. WELL-DEFINED (SINGLE-CRYSTAL) SURFACES

It is widely postulated that atoms on a surface with low lattice coordination numbers, present at defects, serve as the active sites for (electro)catalytic processes. Directly identifying and characterizing the intrinsic activity of these highly localized surface sites would be valuable but is extremely challenging, due to the estimated low coverage, small size, and tendency of these sites to coarsen (restructure) under operational conditions.[7] The electrochemical scanning tunneling microscope has recently been proposed as a promising tool for identifying catalytically active sites at the atomic scale, on the basis of the

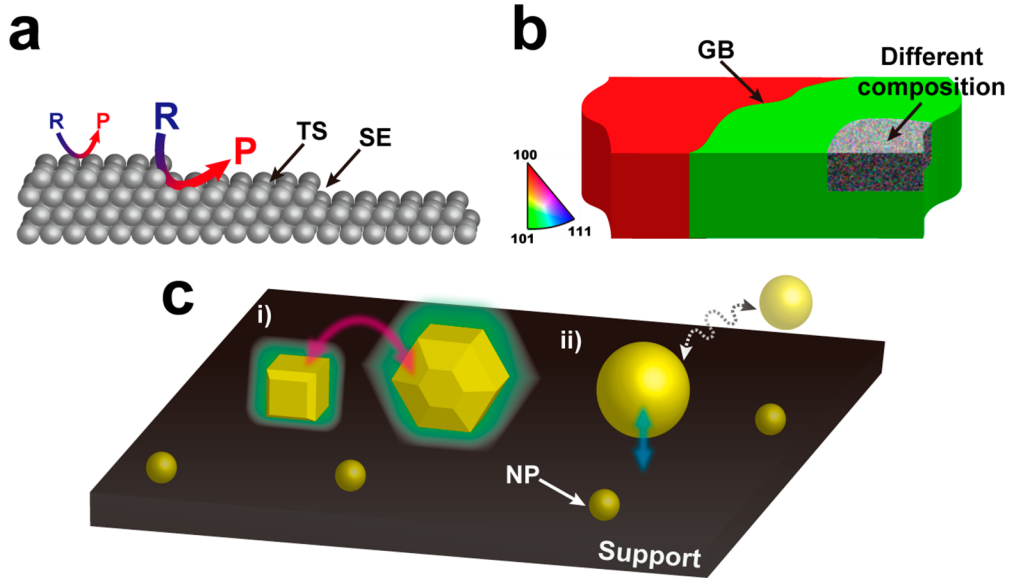

Figure 2. Dynamic (electro)chemical and/or (electro)catalytic processes in action at nanostructured interfaces. (a) Well-defined (single-crystal) surfaces, while nominally structurally and compositionally uniform, as in the terrace site (TS), possess defects such as step edges (SE) that may give rise to nonuniform reactivity and dominate the overall macroscopic response. (b) Extended heterogeneous surfaces, such as polycrystalline metals, comprise structurally (e.g., grains and grain boundaries, GBs) and/or compositionally disparate (e.g., inclusions) sites that can possess vastly different intrinsic electrochemical activities. (c) Nanoparticles (NPs), possessing size-, shape-, and structure-dependent activity, may interact physicochemically (diffusional coupling, aggregation, sintering, etc.) during electrocatalytic turnover (i), as well as undergo dynamic interaction with the support (ii).

DOI: 10.1021/jacs.8b09828
J. Am. Chem. Soc. 2019, 141, 2179−2193

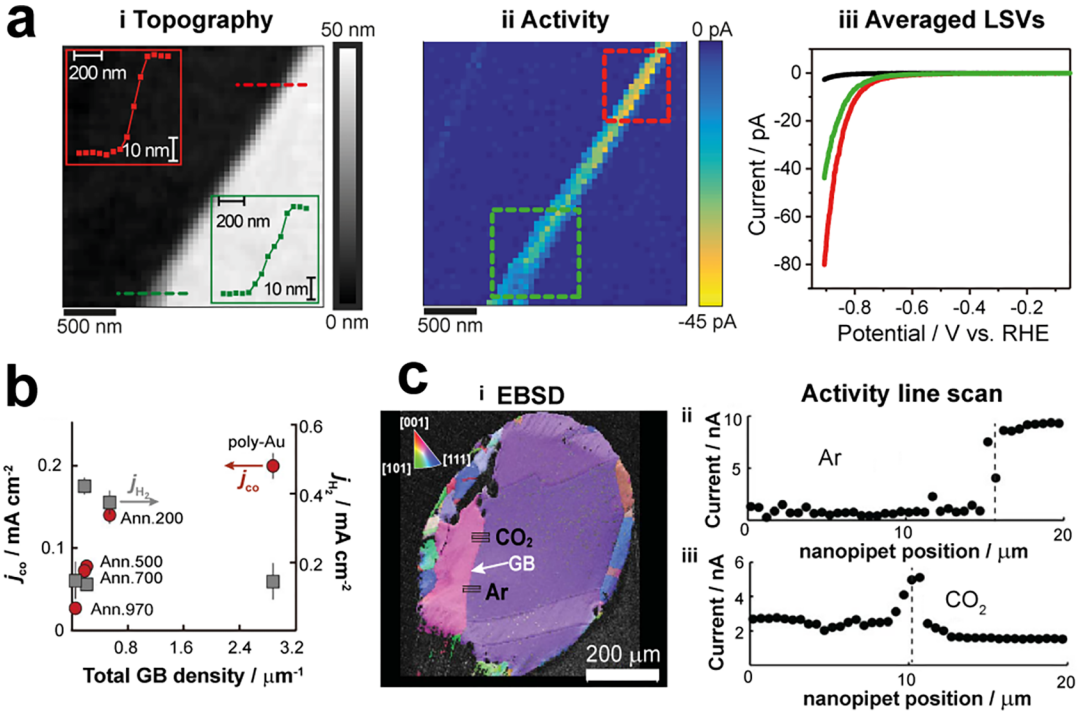

Figure 3. Revealing active sites directly and unambiguously with SECCM. (a) High-resolution (i) topographical and (ii) electrochemical activity maps (−0.857 V vs reversible hydrogen electrode, RHE) obtained with a fine nanopipet probe (tip diameter, $d_t \approx 30$ nm) in the SECCM format, visualizing enhanced HER activity on the edge plane of MoS_2. Insets in (i) are z-height line-scan profiles, showing multilayer surface defects of ca. 21 and 41 nm in height (green and red traces, respectively). (iii) Averaged linear sweep voltammograms obtained on the basal plane (black trace) and surface defects (steps) of ca. 21 nm (green trace) and ca. 41 nm (red trace) in height. Adapted with permission from ref 16. Copyright 2017 American Chemical Society. (b) Bulk electrolysis (−0.4 V vs RHE) partial current densities associated with CO (j_{CO}, red points, left axis) and H_2 (j_{H2}, gray points, right axis) production versus total GB density, obtained on polycrystalline (poly-Au) and a series of annealed (200, 500, 700, and 970 °C) Au foil samples in aqueous bicarbonate media. (c) (i) Electron backscatter diffraction (EBSD) map obtained at an Au wire (diameter ∼500 μm) annealed at 970 °C (colors indicate different grain orientations, legend shows pole figure orientations). Electrochemical activity line scan profiles obtained across the GB labeled in (i) (paths shown inset), performed in the SECCM format under (ii) Ar (HER only) and (iii) CO_2 (CO_2 reduction plus competing HER) atmospheres. The dashed lines in (ii) and (iii) indicate the position of the GB. From ref 18. Reprinted with permission from AAAS.

premise that, under reaction conditions, the electron tunneling barrier will be different over active and nonactive sites[11] (induced by local changes in electrolyte composition or adsorption/desorption processes). In practice, this has been demonstrated by monitoring changes in tunneling current noise to directly identify the active sites at metal single-crystal surfaces. For instance, elevated tunneling current noise ("activity") was identified at steplike defects in comparison to terrace sites for the hydrogen evolution reaction (HER) and oxygen reduction reaction (ORR) on Pt(111) surfaces. Furthermore, this approach revealed elevated HER activity at the boundary regions between monoatomically high Pd islands supported on an Au(111) surface, attributed to the electronic properties of active Pd atoms in the centers of the island and at their boundaries being altered dissimilarly by the catalytically inactive Au substrate.[11]

A second class of materials that can be characterized by long-range order is carbon sp^2 materials (graphite, graphene, and carbon nanotubes), which are widely used and studied electromaterials. Along with the predominant basal surface (or side wall for nanotubes), there are a variety of defects, with the type, concentration, and distribution depending on the source and/or method of synthesis of the material.[12] Identifying the contribution of these different sites to the electrochemistry of carbon electrode surfaces is important, as there had been a longstanding view from classical macroscale electrochemistry that defects dominated the electrochemistry of sp^2 carbon materials, even for simple outer-sphere redox processes (Figure 1a). The advent of nanoscale electrochemical methods, notably scanning electrochemical cell microscopy (SECCM), in tandem with complementary microscopy techniques applied to the same area (notably Raman microscopy and atomic force microscopy) enabled these established hypotheses to be tested by targeting and characterizing key surface features independently for the first time.[12]

In SECCM, electrochemical measurements are performed in a series (typically many thousands) of small areas of a surface defined by a meniscus (droplet) cell created between a nanopipet probe filled with electrolyte solution (mobile electrochemical cell) and substrate (working electrode) surface. During operation, the positions of the nanopipet probe and/or substrate are precisely controlled in 3D space using piezoelectric positioners, and electrochemical (e.g., voltammetric) measurements are performed by applying a potential between a quasi-reference counter electrode (QRCE) located within the probe and substrate surface.[13] The QRCEs used in SECCM (and scanning ion conductance microscopy, SICM; vide infra) are predominantly comprised of electrochemically stable Ag/AgCl wires,[14] although alternative QRCEs such as palladium−hydrogen have also been used,[15−17] in addition to conventional three-electrode formats.[18] A key attribute of SECCM is that it can be viewed through the lens of classical electrochemical methodology, i.e., well-known electrochemical techniques can be applied directly, but in a format where the cell (i.e., working

DOI: 10.1021/jacs.8b09828
J. Am. Chem. Soc. 2019, 141, 2179−2193

electrode area) is orders of magnitude smaller and more mobile, enabling many thousands of local (spatially resolved) electrochemical measurements to be made across a surface, which can be analyzed quantitatively.[19] Additionally, as SECCM is usually carried out under "ambient" conditions (i.e., exposed to air) or under an inert atmosphere, the probe position can be conveniently visualized pre- and/or post-experiment using a camera; this key attribute greatly facilitates colocated ex situ spectroscopic/microscopic analysis, allowing a range of techniques (*correlative multimicroscopy*) to implemented in the same area as SECCM scans.[12]

An illustrative example of the type of measurements that can be made with correlative electrochemical microscopy (i.e., SECCM in conjunction with colocated structural analysis) is the characterization of single-, bi-, and few-layer exfoliated graphene (identified by Raman microscopy), within a single sample on an insulating oxide covered silicon support. The $[Ru(NH_3)_6]^{3+/2+}$ redox process (in aqueous solution) was shown to exhibit layer-dependent electron-transfer kinetics, where the apparent k^0 value scaled with overall layer number.[13] The history (aging) of the sample was also shown to be an important factor governing the electrochemical response of graphene and graphite, with step edges showing enhanced activity in comparison to the basal surfaces on aged samples for the $[Ru(NH_3)_6]^{3+/2+}$ process, in contrast to freshly cleaved highly oriented pyrolytic graphite (HOPG), where the reaction was entirely diffusion limited on the time scale accessible by SECCM.[13,20] These observations were rationalized in terms of the local density of electronic states at these characteristic features, and kinetic data were analyzed semiquantitatively in terms of a Gerischer−Marcus model for heterogeneous electron transfer.[13,21] In a similar fashion, SECCM was able to prove that defect-free regions of the sidewalls of single-walled carbon nanotubes could support fast electron transfer for outer-sphere redox processes and that conducting and semiconducting carbon nanotubes showed contrasting behavior for certain cathodic processes.[12] While defects were not important for simple redox processes, they were shown to be critical for the ORR.[22] An important aspect of many SECCM studies of sp^2 carbon materials has been to show how nanoscale reactivity scales up rationally to explain macroscopic behavior. Consistency in electrochemical data across length scales and time scales, rationally underpinned by surface physics, is a critical theme for the future that needs to become routine in electrochemistry.[12,13,20,22]

Local voltammetric measurements with SECCM have also revealed new insights on structure−activity dynamics in molybdenum disulfide (MoS_2), another class of layered material that has received considerable attention as an earth-abundant HER electrocatalyst.[1,4] Macroscopic electrochemical measurements on ensembles of nanostructured (exfoliated/synthesized) 2H MoS_2 have alluded to high HER activity at the edge plane, owing to the near-thermoneutral free energy of hydrogen adsorption ($\Delta G_H \approx 0$ eV) calculated for this structural element, in comparison to the so-called "catalytically inert" basal plane.[4,23] SECCM was employed to perform current−potential (i−E) measurements on structurally well-defined natural crystals of molybdenite, which were subsequently combined to create electrochemical flux movies over a wide potential range with nanoscale spatial resolution.[15,16] Correlation with complementary structural information from SEM and/or atomic force microscopy revealed uniform HER activity on the basal plane and elevated current densities (i.e., enhanced activity) at the edge plane that scaled linearly with the number of exposed MoS_2 layers (i.e., step height),[15] in line with theoretical predictions and macroscopic electrochemical studies, above.[4,23] For example, in the synchronously obtained high-resolution topography and electrochemical activity maps in Figures 3a-i and ii, the topographical features (corresponding to multilayer step defects) of MoS_2 perfectly align with the areas of elevated surface current, directly (and unambiguously) identifying the edge plane as the active site for HER catalysis, also reflected in the pixel-resolved voltammograms, shown in Figure 3a-iii.[16] The often claimed "catalytically inert" basal plane, which incorporates some surface defects (i.e., sulfur vacancies), was shown to possess a j_0 value comparable to those of moderate HER catalysts (Au and Cu), while the edge plane possessed a j_0 value >10 times larger.[15] It is worth noting that the much higher activity found at the basal surface, particularly in comparison to previous studies on the bulk material,[4] can be explained, at least in part, by the fact that SECCM draws such small currents (typically tens of pA), meaning that it is relatively immune to bulk sample resistance, which is a major problem for macroscopic measurements on resistive semiconductor materials.[12,15,16] Furthermore, for SECCM there is no need to encapsulate the material as an electrode, because the electrochemical meniscus cell is brought into contact with the substrate (working electrode) of interest. In contrast, electrode encapsulation and preparation can also be a practical problem for conventional electrochemical studies of unusual materials (e.g., 2D materials).

These studies[11,13,15,16] and those discussed below clearly demonstrate how scanning probe techniques can go well beyond the capabilities of macroscopic electrochemical measurements to look at the heterogeneities within the surfaces of well-defined metal single crystals[11] and layered materials.[13,15,16] The techniques discussed in this section collect electrochemical and topographical information synchronously (in situ and in real time) which, in conjunction with complementary structural information, reveal nanoscale structure−activity dynamics at functional electrochemical interfaces.

3. EXTENDED HETEROGENEOUS SURFACES

As mentioned in section 1, electrochemical interfaces of practical importance in electrochemistry and (electro)catalysis are structurally and/or compositionally heterogeneous (see Figure 2b). To understand the overall behavior of these complex surfaces, it is essential that structure and activity can be related at the scale of surface heterogeneities. For polycrystalline surfaces, we have introduced a *pseudo single-crystal approach*, where SECCM is used to electrochemically interrogate individual grains and GBs on a polycrystalline surface, which is structurally characterized ex situ with electron backscatter diffraction (EBSD).[24] This approach is being adopted by other groups,[18] and we expect that it should find considerable application in electrocatalysis, as it enables the activity of a wide range of surface features, including high-index facets, which are difficult to prepare as single crystals, and grain boundaries.

This approach is well illustrated by the facet-dependent electrochemistry of $Fe^{2+/3+}$, a well-known outer-sphere process (Figure 1a) with (anion-mediated) inner-sphere routes (Figure 1b),[3] on polycrystalline Pt. In weakly adsorbing electrolyte media ($HClO_4$), the individual (high-index) grains were shown to have markedly different activities, whereas in strongly adsorbing electrolyte media (H_2SO_4), the individual grains exhibited comparable activities, while GBs were highly active,

DOI: 10.1021/jacs.8b09828
J. Am. Chem. Soc. 2019, 141, 2179−2193

dominating the overall surface activity, suggesting that these sites dominate the macroscopic response of polycrystalline Pt. Interestingly, not all GBs exhibited enhanced activity, indicating that the character (geometry) of the GB itself is important (vide infra).[24] The pseudo single-crystal approach has also revealed grain-dependent ORR activity at polycrystalline Pt in acidic media, where SECCM mimics the three-phase boundary of low-temperature fuel cells, with an enhanced flux of O_2 across the meniscus (droplet) cell giving rise to high rates of reactant mass transport. The individual high-index grains were shown to exhibit significantly different ORR activities, while the GBs did not exhibit any enhancement under these conditions.[25]

A very recent study eloquently demonstrated the power of pseudo single-crystal SECCM for rationalizing the macroscopic response of polycrystalline Au for electrochemical CO_2 reduction. Bulk electrolysis data demonstrated increased selectivity for CO production relative to H_2 with increasing GB density (Figure 3b), implying that GBs are more active than the grains for CO_2 reduction but not for the competing HER. This hypothesis was confirmed by SECCM line scanning across a series of GBs with differing geometries (see Figure 3c), where GB-dependent, elevated current (i.e., enhanced activity) was measured at GB surface terminations for CO_2 reduction plus the HER (i.e., enhanced activity at GB relative to the grains under a CO_2 atmosphere; Figure 3c-iii) but not for HER alone (i.e., only grain-dependent activity seen, no GB-specific enhancement under an Ar atmosphere; Figure 3c-ii). The width of the region exhibiting enhanced activity (Figure 3c-iii) was commensurate with the dislocation-induced strain field associated with the each GB, while the degree of enhancement in CO_2 reduction activity was qualitatively consistent with the magnitude of the lattice microstrain, an indicator of the concentration of dislocations within the GB. Thus, GBs create strained regions by stabilizing dislocations, creating high-energy surfaces that are "kinetically trapped" under electrochemical polarization (catalytic turnover).[18] Consequently, mechanical treatments were applied to annealed (polycrystalline) Au foil to artificially increase the GB (dislocation) density, which translated into substantially increased CO_2 reduction activity at the macroscale,[18] demonstrating how a nanoscale understanding of activity can be translated into the rational design of optimal catalysts.

In addition to structural heterogeneity, (electro)materials may possess compositional heterogeneity, arising during synthesis/growth (e.g., inclusions or surface enrichment in metal alloys). SECCM is a promising technique for probing compositionally heterogeneous surfaces, as demonstrated in a recent study of local HER activity on single-crystal iron nickel sulfides (nominally $Fe_{4.5}Ni_{4.5}S_8$), which are highly efficient electrocatalysts in bulk form. SECCM revealed lower activity from the (111) planes of $Fe_{4.5}Ni_{4.5}S_8$ in comparison to bulk macroscale measurements, suggesting that defects in single crystals, which would be exposed in bulk measurements, are largely responsible for the observed macroscopic activity. This was confirmed by performing local measurements on a macroscopic "defect" site, which showed higher activity in comparison ot the basal (111) surface. Local composition was also found to play an important role; Fe-enriched material with segregated regions possessing Fe:Ni ratios higher than the nominal 1:1 exhibited substantially higher activity.[26]

These studies[18,24−26] and others (see below) have effectively demonstrated SECCM as a powerful tool for probing structure-dependent activity and rationalizing the macroscopic response of structurally and/or compositionally heterogeneous electrodes. The pseudo single-crystal approach produces results that are consistent with conventional single-crystal studies at low-index facet electrodes,[24,25] while it also allows high-energy surfaces, such as high-index facets and GBs, to be studied. Moving forward, the high-speed, high-resolution SECCM configuration established in refs 16 and 27 opens up the possibility of probing a larger population of grains (or compositions) in greater detail, where the entire $i-E$ characteristic can be mapped at each point of a heterogeneous electrode surface and combined to create spatially resolved electrochemical flux movies. This information, taken in conjunction with complementary information on the local heterogeneities that give rise to the high activity (e.g., GBs[18,24] or the crystallographic defects/Fe-enriched areas[26]) that dominates the macroscopic (bulk) response of these materials, will enable a more holistic view of the structural and/or compositional controls in (electro)catalysis.

4. NANOPARTICLES ON SURFACES

"Real" electrocatalysts are typically nanostructured, the most common example being NPs (see Figure 2c), which serves to maximize surface area and expose particular surface sites.[1,4,7] As alluded to above, bulk measurements of NPs effectively "wash out" the unique properties of each individual entity within an ensemble, and for this reason there has been a strong drive to develop techniques capable of performing measurements at the single-entity level. Here, we highlight emerging trends in identifying key physicochemical phenomena of NP electrochemistry at the nanoscale.

4.1. Single-Nanoparticle Electrodes. A single NP electrode is the conceptually simplest approach to study electrochemistry at the single-entity level. This approach has many advantages, including well-defined and fast mass transport when the size and geometry of the NP is known: for example, through complementary SEM or transmission electron microscopy (TEM) analysis of the electrode/NP assembly. The benefits of studying single NPs are well illustrated by considering the energy storage and oxygen evolution reaction (OER) properties of individual nonfaceted $Ni(OH)_2$ NPs electrodeposited onto carbon nanoelectrodes.[28] By performing voltammetry at the single-NP level, it was shown that charge storage via the reversible Ni(II)/Ni(III) transformation was diffusion-limited (nonpseudocapacitive) and that the OER kinetics and mechanism (Tafel slope) were invariant with respect to NP diameter in the considered size range (diameter of NP (d_{NP}) 40−1000 nm).[28]

Coupled in situ microscopy adds further benefits to single NP studies, as exemplified by investigations of electrodeposited $Co(OH)_2$ particles (d_{NP} = 0.5−3 μm), where the overall reaction rate (inferred from electrochemical current) was linked to dark-field microscopy measurements of particle size and Co redox state. The reversible Co(II)/Co(III) transformation was shown to coincide with "electrochemical breathing", where the particle undergoes rapid volume expansion and slow volume contraction during the oxidation and reduction processes, respectively.[29]

Ongoing work in this area should focus on the study of structurally well-defined, shape-controlled (faceted) NPs, which can be grown through electrosynthesis (electrodeposition) and characterized using selected area (electron) diffraction. This strategy has been illustrated in a recent study[30] and will be valuable in establishing relationships between structure (i.e., size and/or shape) and activity at the single-NP level.

DOI: 10.1021/jacs.8b09828
J. Am. Chem. Soc. 2019, 141, 2179−2193

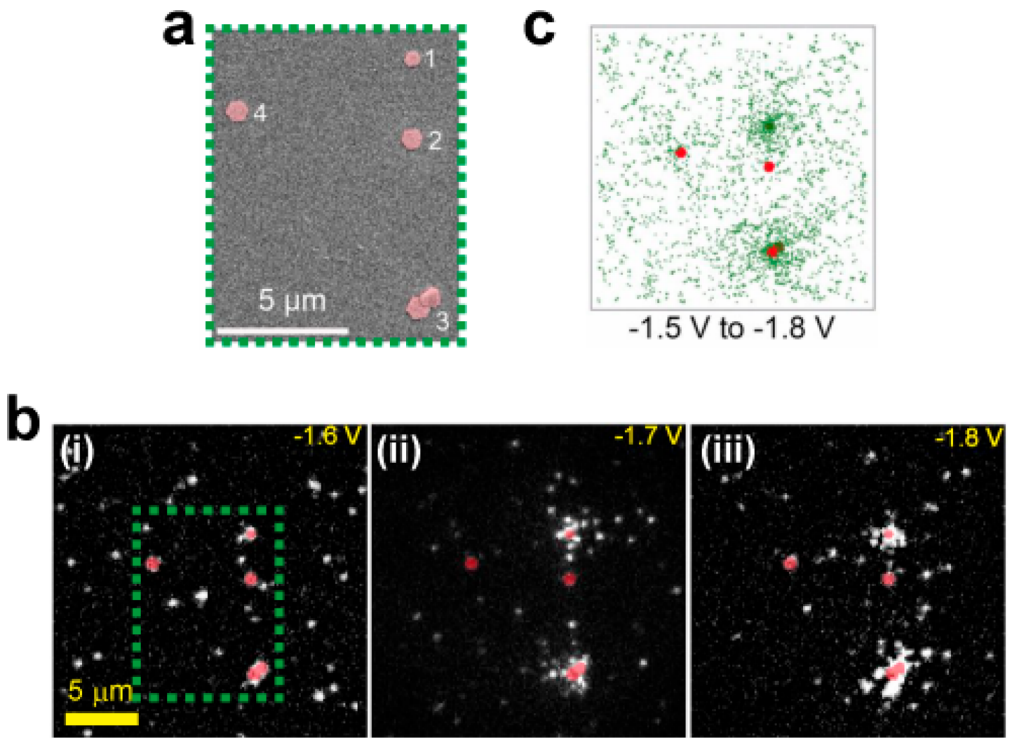

Figure 4. Imaging H_2 nanobubble formation and hydrogen spillover during electrocatalytic HER. (a) SEM image of an Au-nanoplate-modified ITO electrode (individual nanoplates are falsely colored red and labeled 1−4). (b) Total internal reflection fluorescence images showing the dynamic nucleation and growth of H_2 nanobubbles (recognized as the white contrast in the images) at the area of the Au nanoplate-modified ITO electrode shown in (a) at increasingly negative potentials of (i) −1.6 V, (ii) −1.7 V, and (iii) −1.8 V (all vs Pt quasi-reference electrode). (c) Scatter plot showing the accumulated spatial distribution of H_2 nanobubbles in the −1.5 to −1.8 V potential window, where each colored dot represents one detected nanobubble. Adapted with permission from ref 35.

4.2. Local Ensemble Measurements. The single-NP electrode approach is intrinsically low throughput (i.e., single NP at a time) and neglects the influence of the electromaterial support and neighboring NPs. Local ensemble measurements allow a number of individual NPs (or a small population of NPs) to be selected and probed in situ and in a high-throughput manner. The electrochemical characteristics of a single NP within an ensemble can be resolved by detecting changes in the surface refractive index (and thus scattering intensity) resulting from surface electrochemical reactions, leading to optical contrast in surface plasmon resonance images, which are used to derive electrochemical currents and construct local (spatially resolved) voltammograms.[31] This technique, originally used for single-particle electrocatalysis studies,[32] has recently been expanded to obtain the electrochemical i−E profiles and charge/discharge characteristics of single $LiCoO_2$ nanoplates (size of ca. 200 nm) within an ensemble, resolving phase transitions and quantifying Li^+ diffusion rates in situ.[33] To fully elucidate the structural controls on the electrochemical activity of individual entities within an ensemble, it would be interesting to combine plasmonic-based electrochemical current imaging with other high-resolution imaging tools, such as TEM and scanning tunneling microscopy, applied to the same particle.

Super-resolution fluorescence techniques offer a spatial resolution that is not limited by the diffraction of light (typically tens of nanometers).[34] While they are mainly focused on life sciences applications,[34] these techniques are beginning to find use as a probe of electrode activity, as exemplified by a recent study of the HER, where H_2 nanobubbles labeled with fluorescent dye molecules were imaged at individual Au nanoplates supported on an indium tin oxide (ITO) electrode at various potentials, as shown in Figure 4. The bubble nucleation frequency was generally higher on the Au nanoplates in comparison to the ITO support (see Figure 4b), although it should be emphasized that only certain nanoplates exhibited significant HER activity (e.g., nanoplates 1 and 3 versus nanoplates 2 and 4), again highlighting the importance of single (nano)entity studies in rationalizing the macroscopic electrochemical response of an ensemble. Interestingly, a very large number of nanobubbles nucleated within the ca. 3 μm radius of the "active" nanoplates on the ITO surface, particularly at high driving potentials (Figure 4b-ii,b-iii), are clearly evident from the cumulative scatter plot in Figure 4c. This was thought to be a manifestation of the "hydrogen spillover effect", where H atoms generated on the catalyst surface migrate onto the support before undergoing nucleation to form H_2 nanobubbles. This phenomenon is well-known in the gas phase but has rarely been reported in the electrochemical context, with this study being the first example of real-time imaging of electrochemically generated nanobubbles.[35]

A separate approach, and one that works at atomic resolution, is the use of identical-location (ex situ) TEM imaging to monitor structural changes within an ensemble induced by (electro)-chemical perturbation. High-resolution aberration-corrected scanning transmission electron microscopy (STEM), with an electron-transparent conductive boron-doped diamond support, has recently been used to probe the initial stages (0−30 ms) of the nucleation and growth of Au through electrodeposition at high η, progressing from single Au atoms to noncrystalline nanoclusters (AuNCs) through to crystalline AuNPs ($d_{NP} \approx 1$−3 nm).[36] Potential-induced atom movement, atom clustering, and AuNC transformation into crystalline AuNPs, which in

DOI: 10.1021/jacs.8b09828
J. Am. Chem. Soc. 2019, 141, 2179−2193

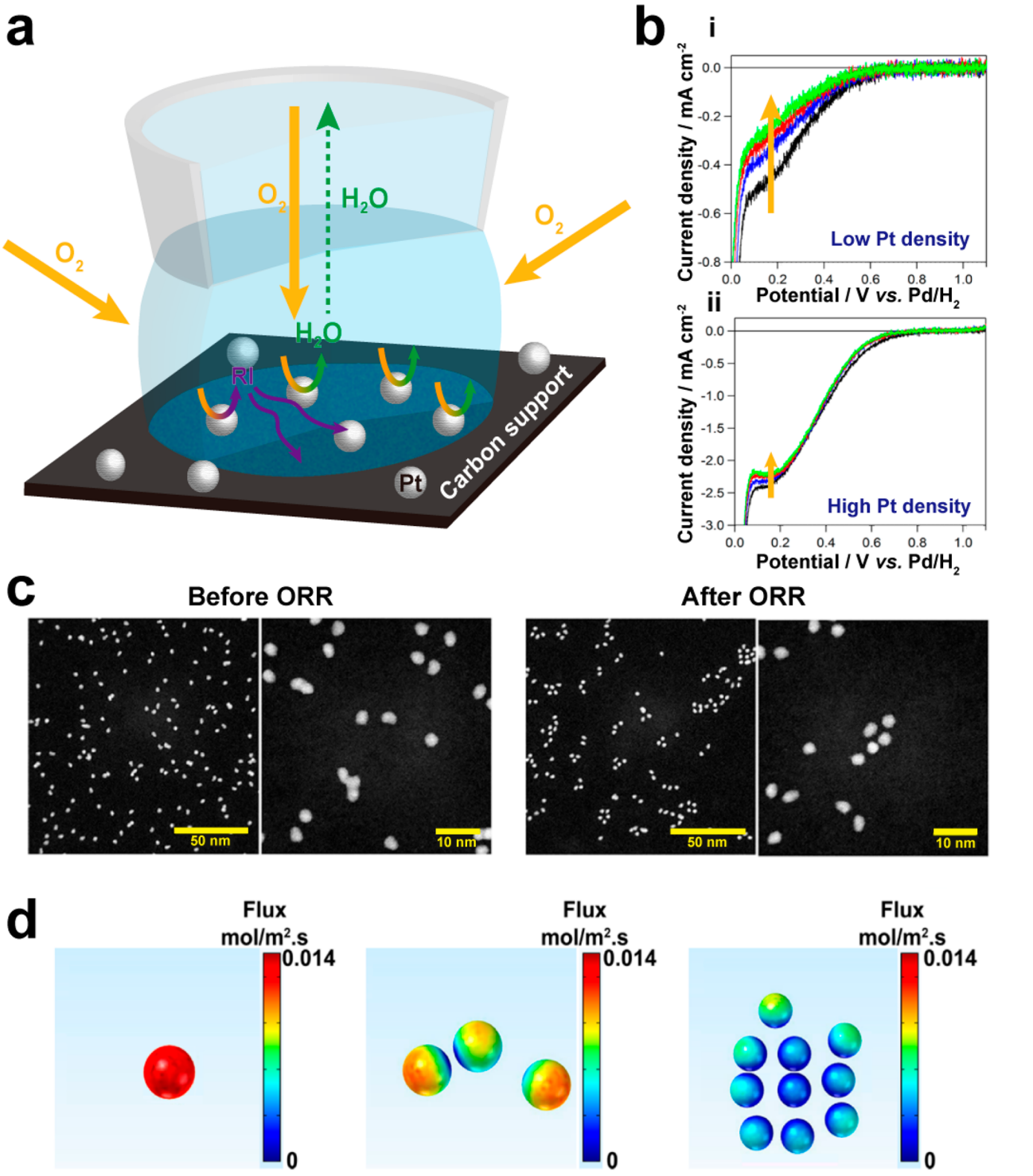

Figure 5. Combining a micropipet droplet cell (SECCM) with ex situ STEM analysis for local ensemble measurements of NCs. (a) Schematic of the end of the nanopipet probe employed in SECCM on a carbon-coated TEM grid (with Pt NCs), showing the flux of reactants (O_2, flux across the meniscus three-phase boundary and down the pipet) and products (H_2O and reactive oxygen intermediates, RIs, flux up the pipet only) in this configuration. (b) Successive linear sweep voltammograms (indicated by the arrow), obtained from (i) low-density (surface coverage ~6%) and (ii) high-density (surface coverage ~37%) PtNC arrays, demonstrating density-dependent progressive catalytic deactivation with potential cycling. (c) STEM images of low-impact-energy deposited PtNCs before and after ORR catalysis (potential cycling), demonstrating the effects of NC migration on ensemble morphology. (d) Flux maps extracted from FEM simulations, revealing the morphology-dependent uneven distribution of flux around individual NCs during catalytic turnover. Adapted with permission from ref 38. Copyright 2018 American Chemical Society.

contrast to classical theory occurs through either loss or gain of atoms, were observed ex situ, with monocrystalline AuNPs being the dominant structure after 30 ms of electrodeposition. Discrete entities (atoms, AuNCs, and/or AuNPs) were also shown to interact during the early stages of electrodeposition via an aggregative growth mechanism,[37] with a strong tendency for disordered AuNCs to be consumed when they were in close

DOI: 10.1021/jacs.8b09828
J. Am. Chem. Soc. 2019, 141, 2179−2193

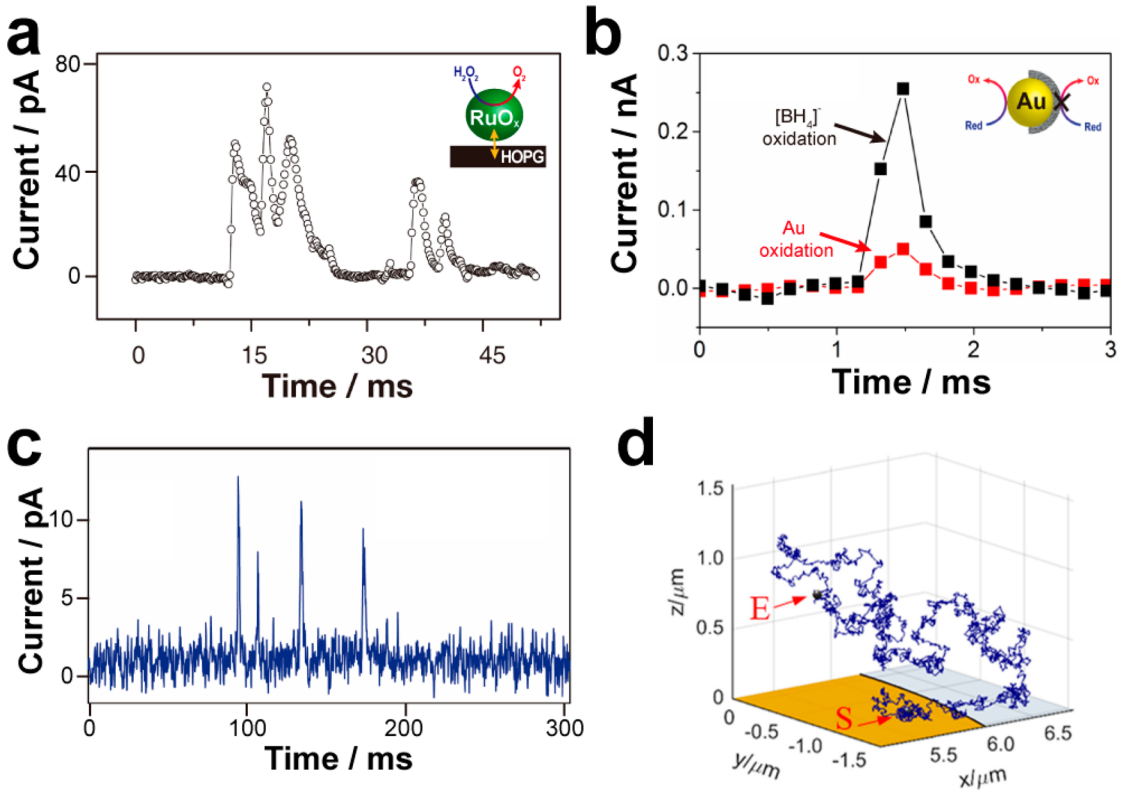

Figure 6. High-bandwidth measurements of electrochemical impact events, revealing dynamic NP−electrode interactions. (a) Multipeak current-time (i−t) response associated with ruthenium oxide NP ($d_{NP} \approx 56$ nm) impact events (detection through electrocatalytic amplification with H_2O_2, inset) at a HOPG collector electrode, measured with a high-bandwidth current follower. Adapted with permission from ref 44. Copyright 2015 American Chemical Society. (b) Rapid i−t response associated with oxide formation (red trace) and catalytic $[BH_4]^-$ turnover followed by deactivation (black trace, deactivation caused by oxide formation, inset) at a single AuNP ($d_{NP} \approx 39$ nm). Adapted with permission from ref 45. Copyright 2016 American Chemical Society. (c) Multipeak i−t response associated with the oxidative dissolution ("partial stripping") of single AgNPs ($d_{NP} \approx 60$ nm) at a GC collector electrode. Reproduced from ref 46 with permission from the Royal Society of Chemistry. (d) Simulated trajectory (time scale 100 ms) of an AgNP ($d_{NP} = 70$ nm) undergoing multicollisional partial oxidations over an Au collector electrode. The yellow and gray regions at $z \approx 0$ μm represent the electrode and glass sheath, respectively. Start and end positions are indicated by S and E, respectively. Reprinted with permission from ref 49. Copyright 2017 American Chemical Society.

vicinity to ordered AuNPs, which transitioned through a disordered state first, before undergoing recrystallization.[36]

Pipet probes have been employed to perform local ensemble measurements, as demonstrated in a recent study[38] where SECCM was used to investigate the ORR response of a small population ($N < 16000$) of size-selected Pt nanoclusters (PtNCs, $d_{NC} \approx 3$ nm) deposited onto a carbon-coated TEM grid support, under high mass transport rate conditions (O_2 flux across the meniscus;[25] see Figure 5a). At low surface coverages, the activity decreased with successive electrochemical (voltammetric) measurements (Figure 5b−i), attributed to poisoning of the PtNCs by carbon- and oxygen-containing moieties that are produced by the reaction of reactive oxygen intermediates (RIs) generated transiently in the ORR with the carbon support (i.e., carbon corrosion). This was less of an issue at high surface coverage, where the distance between clusters was small, meaning that RIs could be either be consumed at the same PtNC (mass transport to individual particles is lower at high coverages) or diffuse to neighboring PtNCs and undergo further reduction, rather than react chemically with the support (Figure 5b-ii). The impact energy during PtNC deposition (achieved with a cluster beam source) also drastically affected NC stability during electrocatalysis, with low-impact-energy PtNCs migrating as a result of ORR, as seen by STEM imaging (see Figure 5c). This migration was attributed to electrochemical propulsion caused by an uneven flux distribution around individual PtNCs within the ensemble, explored through finite element method (FEM) modeling (Figure 5d). The random distribution of PtNCs gives rise to uneven flux, depending on the degree of shielding by neighboring clusters (see Figure 5d), which results in nonuniform electric fields and/or chemical gradients.[38]

SECCM coupled with the use of a TEM grid substrate (explored further below) is a high-throughput approach to performing local measurements on ensembles of true catalytic NPs, strengthened by the capability of performing ex situ structural characterization with STEM and complementary quantitative analysis with FEM modeling. This approach is generally applicable to any (electro)catalytic system. Future work in this area may head in many directions: e.g., to resolve structure−activity in nanostructured energy storage materials or to elucidate support effects on activity, migration, and deactivation of NPs.

4.3. Electrochemical Nanoparticle Impacts. A popular approach for observing the electrochemical properties of single NPs that has gained considerable interest, as highlighted in recent reviews,[39] is to monitor NP impact (or landing) from a solution (colloidal suspension) onto a collector electrode surface (Figure 2c-ii), with detection based, for example, on blocking of the collector current,[40] electrocatalytic amplification at the NP,[41] or oxidative dissolution (stripping) of the NP.[42] NP

DOI: 10.1021/jacs.8b09828
J. Am. Chem. Soc. 2019, 141, 2179−2193

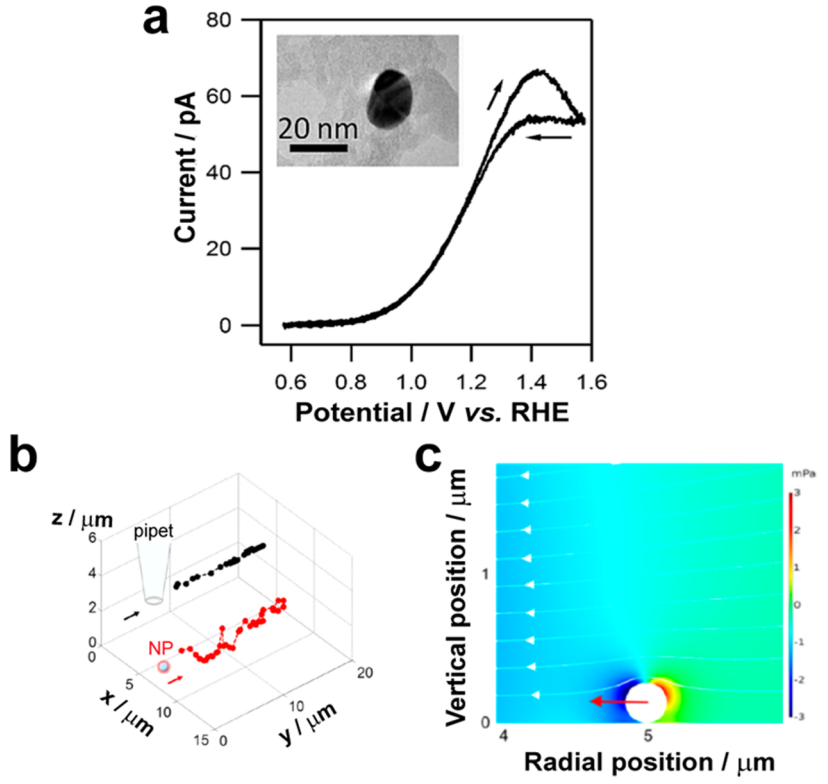

Figure 7. Delivery and manipulation of NPs near (electrochemical) interfaces using pipets. (a) CV obtained from the oxidation of $[N_2H_5]^+$ at a single AuNP, delivered from a micropipet to a carbon-coated TEM grid substrate. The inset is a TEM image obtained ex situ, after electrochemical impact. Adapted with permission from ref 50. Copyright 2012 American Chemical Society. (b) Controlled delivery and manipulation of a NP at an ITO substrate surface, where a potential of 1 V vs Ag/AgCl was applied to "trap" the NP in the vicinity of the substrate, while a negative differential pressure was applied at the pipet to drag the particle along the surface. The 3D trajectories of the pipet (controlled with a piezoelectric positioner) and NP (tracked with superresolution fluorescence microscopy) are shown in the black and red traces, respectively. (c) Simulated pressure profile near a "surface-trapped" NP, where the pipet orifice is located at a radial position of 0 μm. The white streamlines (right to left) indicate the directions of flow, and the red arrow represents the direction of the force on the NP. Reprinted with permission from ref 54. Copyright 2017 American Chemical Society.

impacts are intrinsically fast (beyond the time scale of conventional instrumental amplifiers[43]), and recent works have highlighted the importance of the measurement device bandwidth and data filtering when the $i-t$ transients associated with electrochemical impact events are interpreted.

An important question in this field is whether NPs arriving at an electrode undergo a single-pass interaction (hit and stick or hit and bounce) or undergo multiple interactions. Multiple interactions of a single NP were first exemplified in the study of ruthenium oxide NP impacts on HOPG, detected through the electrocatalytic oxidation of hydrogen peroxide (H_2O_2), where multiple $i-t$ events associated with a single (stochastic) NP impact were detected (i.e., "multipeak" behavior on the microsecond time scale; see Figure 6a). The multipeak behavior was attributed to NPs becoming hydrodynamically trapped in the vicinity of the collector electrode (HOPG) surface and undergoing multiple impacts before release and semiquantitatively reproduced through 3D random walk simulations.[44] High-bandwidth measurements are able to probe even faster processes during electrochemical impact, as demonstrated for oxide formation and associated catalytic deactivation of AuNPs impacting with a collector electrode. The $i-t$ transient associated with AuO_x formation on AuNPs lasts ca. 500 μs (Figure 6b), and the femtocoloumb charge passed in these events is proportional to the AuNP surface area, enabling accurate electrochemical size analysis, with results comparable to those of TEM.[45]

The importance of bandwidth was further emphasized in a study on AgNP dissolution dynamics. By opening of the time window, studies from three different groups revealed that AgNP stripping (oxidative dissolution) was a complex, NP-size-dependent phenomenon, where larger AgNPs undergo multiple and repetitive stripping events (impacts), resulting in often incomplete electrodissolution on the microsecond time scale (a representative example is shown in Figure 6c),[46−48] contrary to original reports.[42] Long and co-workers developed a semi-quantitative 3D random walk model to rationalize the size-dependent multipeak stripping behavior of AgNPs during electrochemical impact, where the trajectories of the AgNPs were described by Brownian motion in bulk, hindered diffusion (hydrodynamic trapping) as well as electric-field-driven motion in the near-wall (electrode) region and size-dependent adsorption/desorption of the AgNP in the electron-tunneling region, where electrodissolution occurs.[48]

White, Zhang, and co-workers attributed the multipeak impact behavior (e.g., Figure 6c) to a single AgNP moving in and out of contact with the collector electrode during a collision event, where the motion of an AgNP at the collector electrode/solution interface was driven solely by Brownian motion.[47] They developed a 3D lattice random walk simulation of AgNP Brownian motion dynamics (based on mass-dependent thermal velocity) in the near-electrode region (Figure 6d), which in combination with electrochemical kinetic parameters (i.e., j_0 for the Ag/Ag^+ process) quantitatively reproduced the experimental

DOI: 10.1021/jacs.8b09828
J. Am. Chem. Soc. 2019, 141, 2179−2193

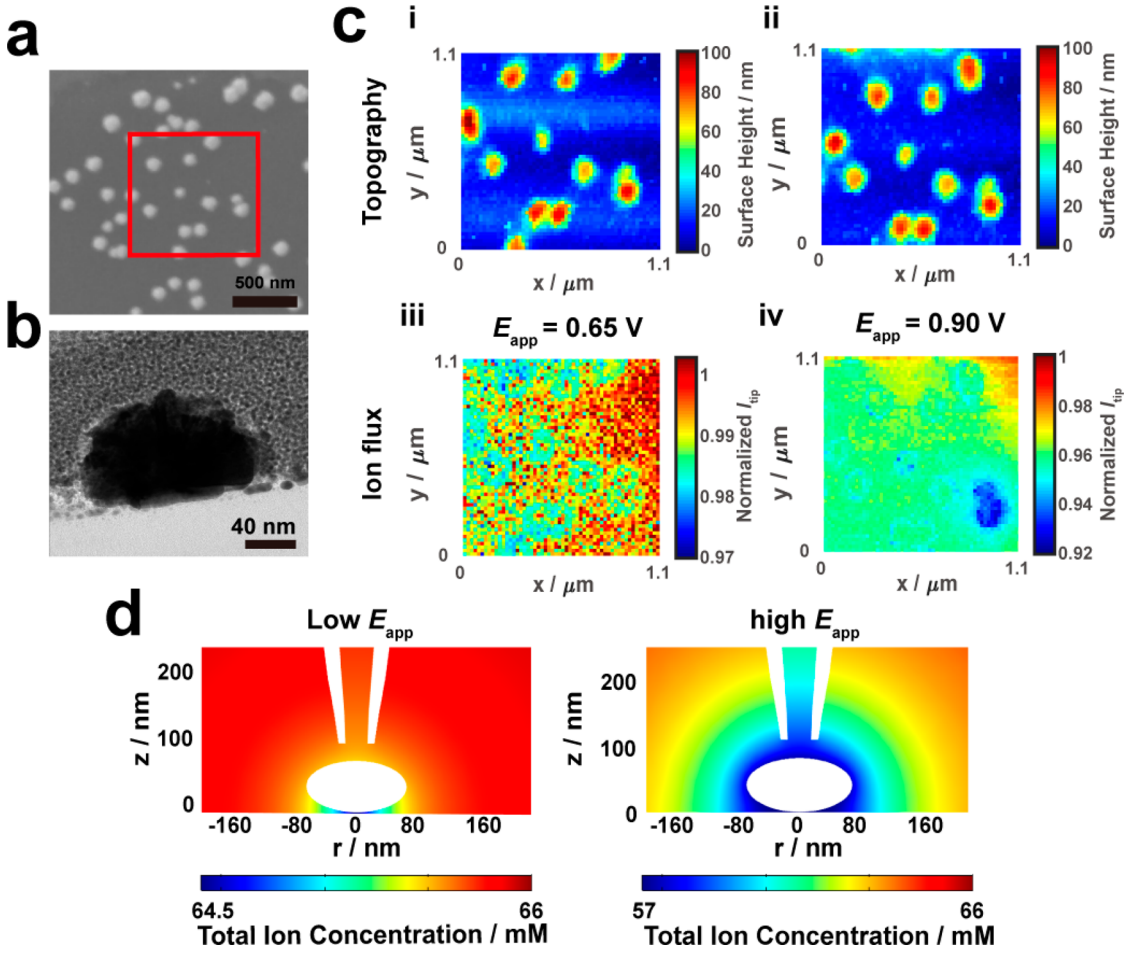

Figure 8. High-resolution, synchronous topographical and electrochemical flux mapping with SICM. (a) SEM image of AuNPs supported on carbon fiber. (b) TEM image of the cross-section of an individual AuNP, showing the NP−support gap that gives rise to hindered mass-transport effects. (c) Topographical (i, ii) and synchronously recorded electrochemical activity images (iii, iv) obtained during catalytic $[BH_4]^-$ turnover at supported AuNPs (mapped area indicated by red box in (a)). The applied potential (E_{app}) is indicated in (c-iii) and (c-iv). These images allow important characteristics of the ensemble to be directly visualized, including geometrical effects (e.g., "ring effect" in (iii)), diffusional overlap, competition between neighboring NPs and heterogeneous NP activity (e.g., bottom-right, "blue" AuNPs in (c-iv)). (d) FEM simulations showing the distribution of ions around an isolated NP during $[BH_4]^-$ turnover with high and low E_{app} (i.e., high and low η). Depletion of ions in the NP−support gap (see (b)) at low E_{app} gives rise to the experimentally observed "ring effect" seen in (c-iii). Adapted with permission from ref 17. Copyright 2017, American Chemical Society.

multipeak and partial stripping behavior. The simulations reveal that tens to thousands of NP−electrode collisions (nanosecond time scale) contribute to experimentally measured peak currents, and suggest that NP thermal velocity controls the electron-transfer rate during electrochemical impact.[49]

By adoption of the highest possible bandwidth measurements, the field of electrochemical impacts has progressed by providing a wealth of information that was obscured in earlier $i-t$ collision transients.[41,42] These improved data highlight single-NP activity,[44,45] motion,[47,48] and surface-interaction dynamics,[44,46] all of which are important in the context of understanding both individual NP activity and the stability and dynamics in NP ensembles (Figure 2c). However, it has to be recognized that interpretation of $i-t$ traces alone can be somewhat ambiguous, necessitating the implementation of complementary microscopy and/or spectroscopy techniques to understand the dynamic redox behavior at the electrode/solution interface during NP impact. For this reason, SECCM was used to deliver single NPs to a catalytically inert carbon-coated TEM grid substrate, used as a working electrode for impact studies, followed by ex situ morphological analysis of collected NPs with TEM. This approach was applied to study the catalytic properties of AuNPs for hydrazinium ($[N_2H_5]^+$) oxidation, where the entire $i-E$ response was measured at the single-NP level (representative example in Figure 7a).[50]

An important advance has been to monitor single NP impacts in situ with a range of optical methods, including 3D super-resolution holographic microscopy, where individual AgNP stripping events are observed in real time. In the absence of complexing/precipitating agents, AgNP stripping is a rapid process but may not take place immediately upon the NP entering the vicinity of the near-electrode region, with a small "lag time" often observed. In the presence of complexing/precipitating agents such as SCN^-, charge injection ($Ag(s) \rightarrow AgSCN(s)$), detected electrochemically, was followed by slow dissolution ($AgSCN(s) \rightarrow [Ag(SCN)_{x+1}]^{x-}$), observed optically but "invisible" electrochemically. In other words, the onset of AgSCN(s) dissolution was delayed relative to the electrochemically detected $i-t$ transient associated with AgNP oxidation.[51] An innovative nanochannel cell configuration has also been developed to optically monitor the dynamic collision and

DOI: 10.1021/jacs.8b09828
J. Am. Chem. Soc. 2019, 141, 2179−2193

oxidation of AgNPs in situ using single-particle fluorescence microscopy.[52]

A further important development in the NP impact field has been the improved delivery of NPs to electrified interfaces using nanopipets, as illustrated by the local delivery of NPs (polystyrene) using a combination of SICM for positioning (vide infra), pressure-driven flow for controlled delivery (with the delivery event sensed through a resistive-pulse method[53]), and super-resolution fluorescence microscopy for imaging NP dynamics. The trajectory was tracked in 3D space and manipulated by balancing the attractive/repulsive forces exerted on the NP by convection and the electric field. NP diffusion kinetics were analyzed to reveal subdiffusive (hindered) motion, resulting from (potential-dependent) attractive electrostatic interactions between the NP and an ITO substrate, or superdiffusive (directed) motion, resulting from pressure-driven flow (convection) at the pipet. This was exploited to manipulate NP position in *real time* with tens of nanometers precision, achieved by moving the nanopipet laterally across the surface while "dragging" the NP along by fluid flow (negative differential pressure; see Figure 7b). FEM modeling was employed to quantify and visualize the distribution of forces impinged upon a near-surface NP ("trapped" by the electric field) as a result of pressure-driven flow (Figure 7c), rationalizing the real-time manipulation of NP motion.[54] This study highlights the significant progress that has been made in the study of NP impacts in terms of sophistication, control, and analysis, in comparison to the original attempts in this field. Together with other studies highlighted, there is a new course for NP impact studies that are most effective when combining high-bandwidth electrochemical measurements, NP sizing (on the fly), and/or microscopy, including in situ optical methods, in order to tease out several phenomena that contribute to the current−time−potential response.

4.4. Electrochemical Imaging. As discussed in section 3, electrochemical imaging is a powerful technique for mapping spatially heterogeneous activity at complex (heterogeneous) electrochemical interfaces. Among a limited set of techniques for nanoscale electrochemical flux mapping, scanning electrochemical probe microscopy (SEPM) techniques (i.e., those using a physical probe), most commonly scanning electrochemical microscopy (SECM), have attracted significant interest. A very recent review covers the efforts on the use of SECM and hybrid techniques in this area, and hence it will not be covered here.[55]

In comparison to the solid nanoelectrodes used in SECM, which can be difficult to make and are susceptible to damage, nanopipets are easily fabricated, even with nanometric dimensions, and produce a robust (unchanging) electrochemical response over extended time periods (hours to days), making them ideal for electrochemical imaging at the nanoscale. Indeed, building on a previous study,[56] it was recently demonstrated how fine nanopipet probes could be deployed in the SICM format for synchronous nanoscale reaction-topography mapping.[17] In SICM, the tip of a nanopipet containing a QRCE (e.g., Ag/AgCl; vide supra) is immersed in bulk solution, where another QRCE is located, and a potential bias is applied between these QRCEs to induce an ion conductance current through the orifice of the pipet. The ion conductance current is sensitive to the access resistance of the nanopipet, which is governed by the tip−substrate distance (i.e., topographical mapping in conventional SICM) in addition to surface charge,[57,58] as well as ion flux arising from (electro)chemical reactions at the interface.[17,56] Through careful control of the SICM probe bias, it is possible to map topography and surface activity simultaneously.

In SICM reaction mapping,[17,56] the probe acts as a "mobile ion conductance sensor", mapping the heterogeneous flux arising from an electrochemical reaction. This aspect is exemplified through studies of the oxidation of $[BH_4]^-$ at carbon-fiber-supported AuNPs (see Figure 8a,b), which consumes OH^-, leading to a local change in ionic composition, while also mapping topography with high fidelity (see Figure 8c-i,c-ii). Ion flux heterogeneities arising from geometrical effects (i.e., NP−support gap, Figure 8c-iii), diffusional overlap, competition for reagent between neighboring NPs (arising due to random distribution of NPs in the ensemble[38]), and differences in NP activity (e.g., bottom-right AuNPs in Figure 8c-iv) were visualized and quantified. FEM modeling (Figure 8d) was employed to rationalize the heterogeneous ion fluxes measured experimentally, with hindered mass transport at the NP−support gap (Figure 8b) giving rise to the characteristic "ring" effect in the activity maps at low driving force (E_{app}, e.g., see Figure 8c-iii).[17]

Nanopipets can also be deployed in the SECCM format to perform direct high-speed, high-resolution electrochemical imaging, as demonstrated for mapping the OER activity of iridium oxide (IrO_x) NPs on a HOPG support. Heterogeneity in OER activity was observed, with some IrO_x NPs possessing considerable activity before the onset of detectable current from the whole ensemble (all NPs plus the support).[59] The high-speed, high-resolution voltammetric SECCM approach established in refs 16 and 27 (e.g., see Figure 3a) has also been used to elucidate the spatially resolved i−E behavior of individual nonfaceted polycrystalline AuNPs ($d_{NP} \approx 350$ nm) grown on a glassy-carbon support. While different individual AuNPs exhibited very similar overall catalytic activity toward $[N_2H_5]^+$ oxidation (at the interparticle level), electrochemical reaction rates varied significantly across the surface of individual AuNPs (at the intraparticle level), attributed to structural (crystallographic) heterogeneities, demonstrating that these single entities cannot be considered uniformly active.[16]

Recent advances in the speed and/or resolution of nanopipet-based SEPM (e.g., SICM[17,56] and SECCM[16,27,59]) has enabled high-fidelity synchronous topographical/electrochemical mapping with true nanoscale (tens of nanometers) resolution. In all of the imaging studies highlighted above,[16,17,27,59] nonuniform electrochemical activity was identified within populations of nominally identical NPs, alluding to structural and/or compositional heterogeneities within the ensemble. Looking to the future, applying nanometer-resolution SEPM with complementary high-resolution spectroscopy/microscopy, e.g., through the use of TEM grid substrates in SECCM,[38,50] will be a powerful approach for (nano)material structure−activity determination, which is a crucial step in rational (electro)catalyst design and synthesis.

Single-particle reactivity mapping (at the inter- and intraparticle levels) has also been achieved with a range of super-resolution (vide supra) optical approaches, which imply (electro)chemical reactivity from the "on/off" states of redox-reporter molecules (oxidized/reduced forms switch between "emissive" and "dark" states) and separately use supplementary techniques to characterize morphology. For example, super-resolution surface-enhanced Raman scattering (SERS) has been used to probe local surface potentials on colloidal Au aggregates labeled with Nile Blue A. Correlation of potential-dependent

DOI: 10.1021/jacs.8b09828
J. Am. Chem. Soc. 2019, 141, 2179−2193

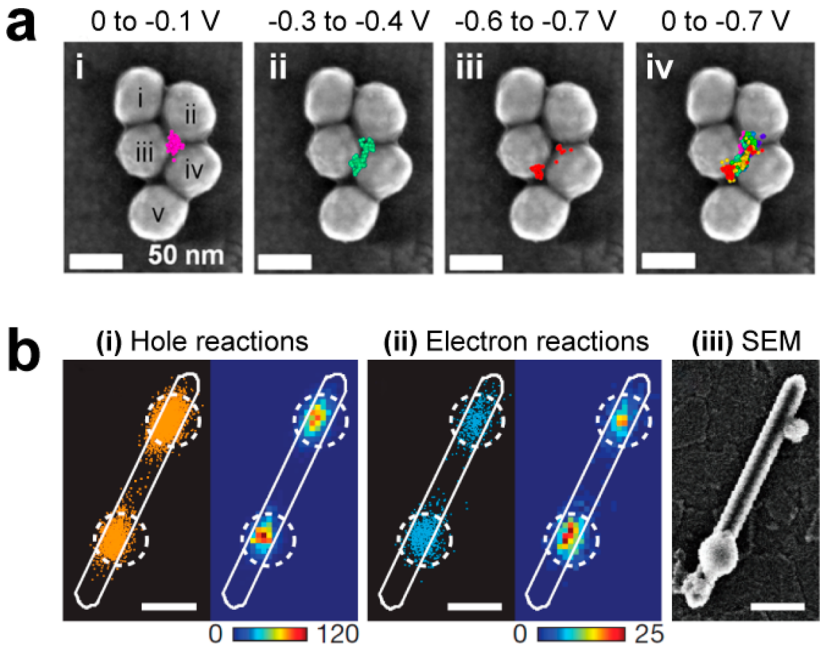

Figure 9. Single-entity (NP) electrochemical activity mapping with superresolution optical techniques. (a) SERS emission centroids (colored dots) as a function of applied potential (all vs Ag/AgCl) (i) 0 to −0.1 V, (ii) −0.3 to −0.4 V, (iii) −0.6 to −0.7 ,V and (iv) 0 to −0.7 V, from an Nile Blue A labeled Au pentamer, overlaid on the corresponding SEM image. The emission centroids, initially located at the geometric center of the pentamer (i), spreads out (ii) and becomes localized at two junctions at increasingly negative potential (iii), indicating spatially dependent reduction potentials (iv). Reprinted with permission from ref 60. Copyright 2015, American Chemical Society. (b) Scatter plots (left image in (i) and (ii), each orange or blue dot represents a single event) and 2D histograms (right image in (i) and (ii), scale bar indicates number of events) of individual single-molecule fluorescence events, reflecting (i) hole- and (ii) electron-driven surface reactions (product is resorufin, a fluorophore) on a TiO_2 nanorod. (iii) SEM image of the TiO_2 nanorod in (i) and (ii) after decoration with an OER catalyst (cobalt-borate). Reprinted by permission from ref 62. Copyright 2016, Macmillan Publishers Ltd.

emission centroids with morphological information from SEM revealed that there were discrete locations, typically situated at NP−aggregate junction regions, associated with the reporter molecules that were most difficult to reduce/easiest to oxidize. In other words, at high potentials, when all Nile Blue A molecules are in the emissive (oxidized) state, the emission centroid is initially located at the geometric center of the AuNP-aggregate (Figure 9a-i), before spreading out (Figure 9a-ii) and becoming localized at specific junctions (Figure 9a-iii) at increasingly negative potentials. From this, it was hypothesized that reporter molecules at certain locations experience site-specific electrochemical environments (Figure 9a-iv) or location-dependent redox potentials.[60]

Super-resolution single-molecule fluorescence microscopy has been employed for (electro)chemical imaging, e.g., for mapping spatiotemporal fluctuations in single-molecule catalysis events on Sb-doped TiO_2 nanorods, where the middle of the nanorod was shown to be more active initially for OER photocatalysis, before deactivating (but sometimes recovering in a "self-healing" mechanism), causing the two ends of the rod to dominate the overall activity in the time-integrated response, despite lower intrinsic activity.[61] The same technique has also been used to probe intraparticle photoactivity on pristine and catalyst-modified single-crystal rutile TiO_2 nanorods supported on ITO, under an applied potential bias. Hole- and electron-induced surface reaction rates were shown to be strikingly nonuniform along the surface of single nanorods, with a strong spatial correlation between the hole (Figure 9b-i)- and electron-induced (Figure 9b-ii) photocatalytic "hot spots", revealed to be structural defects or impurity sites from complementary ex situ TEM/SEM analysis. The photocurrent associated with OER (i.e., photocatalytic activity for water oxidation), measured through the ITO substrate upon local laser illumination, revealed that the catalytically active sites coincide with the hole- and electron-driven "hot spots" (Figures 9b-i,b-ii, respectively), indicating that these sites effectively mediate both oxidation and reduction reactions. The TiO_2 nanorods were subsequently decorated with an OER catalyst (cobalt-borate) through local photodeposition (Figure 9b-iii), which enhanced hole-/electron-driven photoelectrocatalytic activity at initially low activity sites and/or lowering the onset potential of the OER, especially at sites with initially high onset potentials. These two types of sites are not necessarily the same, highlighting the challenge of engineering efficient photoanodes with minimal amounts of catalyst, and on this basis, a block−deposit−remove type strategy to yield optimally located catalysts was proposed.[62]

Super-resolution optical approaches have revealed active "hot spots" directly at the single-molecule level[60−62] of NPs in the hundreds of nanometers size range, as well as enabling studies of the time evolution of (electro)catalytic activity[62] and catalytic cooperativity in real time.[10] These techniques are undoubtedly very powerful, achieving unprecedented spatial (tens of nanometers) and temporal (sub-microsecond) resolution, but are restricted to the use of certain materials (i.e., plasmonic materials in surface plasmon resonance) and probe molecules (e.g., redox fluorophores in single-molecule fluorescence), as well as optically transparent supports. In contrast, scanning probe methods, such as SICM and SECCM outlined above, are more generally applicable to any class of (electro)catalytic system and provide synchronous topographical (morphological) information but are generally carried under true catalytic

DOI: 10.1021/jacs.8b09828
J. Am. Chem. Soc. 2019, 141, 2179−2193

turnover conditions, rather than the single-molecule level, making cross-correlation between temporally neighboring catalytic events[10] impossible. While significant recent advances in this area have enabled nonuniform (electro)chemical fluxes to be measured at the sub-100 nm level, electrochemical imaging techniques alone generally cannot unambiguously reveal the compositional and/or structural origin of the nonuniformity, which must come through *correlative multimicroscopy*, in which electrochemical images and movies are related to colocated images of surface structure, chemistry, and/or electronic properties. This versatile philosophy, highlighted and emphasized throughout this Perspective, needs to be adopted more widely in the future in order to resolve the relationship between surface structure and activity in electrochemistry and electrocatalysis.

5. SUMMARY AND OUTLOOK

In this Perspective we have highlighted recent approaches to studying fundamental electrochemistry and electrocatalysis, whereby colocated information on structure and activity is collected on commensurate scales, ranging from hundreds of nanometers all the way down to the atomic level. Some of the different techniques that we have discussed provide electrode topography and activity synchronously, and although this alone may reveal a wealth of information, there is often the need to further employ complementary ex situ high-resolution microscopy/spectroscopy, which for some techniques (e.g., SECCM) is easier to implement due to the ease of obtaining a wide field optical view pre-/post-experiment but for others may require sample marking to assist in the use of colocation techniques. This correlative electrochemical multimicroscopy approach avoids the ambiguity inherent to classical macroscopic or bulk electrochemical techniques, where the electrochemical response is averaged over a large population of interacting surface sites, obscuring the nature of key elementary processes.

We have covered well-defined (single-crystal) surfaces (section 2), structurally and/or compositionally heterogeneous extended surfaces (section 3), and complex NP/support ensemble-type electrodes (section 4). While each configuration presents a unique set of challenges in terms of structure−activity resolution, one important aspect we have emphasized throughout is the importance of targeting the characteristic "single entities" that make up these electrochemical interfaces, to enable multiscale predictions that link the microscopic and macroscopic worlds. Another important aspect borne out of these studies is the importance of applying theory and developing computational models/simulations to rationalize experimental data, a combined approach that is becoming more accessible with the availability of powerful commercial software packages. Indeed, it is the consistency between experiment and theory at the single-entity (nanoscopic) level that allows macroscopic (bulk) behavior to be explained and further predicted, enabling materials discovery and the rational design of improved functional materials for technologically important applications such as energy conversion and storage.

Future avenues for high-resolution structure−activity measurements in electrochemistry that promise a holistic view of electrode dynamics will include improved in situ and in operando imaging techniques that incorporate electrochemical microscopy alongside other forms of microscopy, the integration of spectroscopic capability into imaging probes to enhance chemical information, the use of "intelligent probes" that make use of AI and machine learning, and methodologies that draw on the convergence in the scale of measurements and molecular dynamics and density functional theory simulations. There is no doubt that the techniques and technologies will continue to push the state of the art in terms of spatiotemporal resolution, measurement speed, and multifunctionality, enabling the routine study of phenomena on smaller length scales: for instance, catalytic sites at the atomic level (e.g., single-atom step defects[11]) or mapping of local electrical double-layer properties (i.e., surface charge[57,58]). Multifunctional, spatiotemporally resolved, and multilength scale studies inevitably generate large volumes of data, also necessitating the development and adoption of big data mining protocols in this field. We have only just scratched the surface of what is possible with single-entity electrochemistry and correlative electrochemical microscopy, but it is important not to lose sight of the importance of "ease of use" and "user friendliness"; future developments will also need to make the technologies accessible to the "general user" in order to facilitate the widespread adoption of these powerful techniques and methodologies.

AUTHOR INFORMATION

Corresponding Authors

*E-mail for C.L.B.:C.Bentley.1@warwick.ac.uk.
*E-mail for P.R.U.: P.R.Unwin@warwick.ac.uk.

ORCID

Cameron L. Bentley: 0000-0001-7867-6068
Minkyung Kang: 0000-0003-3248-8496
Patrick R. Unwin: 0000-0003-3106-2178

Notes

The authors declare no competing financial interest.

ACKNOWLEDGMENTS

C.L.B. acknowledges financial support from the European Union's Horizon 2020 research and innovation programme under the Marie Skłodowska-Curie grant agreement No. 702048 (NEIL) and the Ramsay Memorial Fellowship Trust. P.R.U. gratefully acknowledges support from a Royal Society Wolfson Research Merit Award.

LIST OF SYMBOLS

Symbol	Meaning
d_{NP}	diameter of nanoparticle
d_t	tip diameter
E	potential
$E^{0\prime}$	formal reduction potential
i	current
j	current density
j_0	exchange current density
k^0	standard rate constant
α	transfer coefficient
η	overpotential

LIST OF ABBREVIATIONS

Abbreviation	Meaning
EBSD	electron backscatter diffraction
FEM	finite element method
GB	grain boundary
HER	hydrogen evolution reaction
HOPG	highly oriented pyrolytic graphite
ITO	indium tin oxide
NC	nanocluster
NP	nanoparticle

DOI: 10.1021/jacs.8b09828
J. Am. Chem. Soc. 2019, 141, 2179−2193

OER	oxygen evolution reaction
ORR	oxygen reduction reaction
QRCE	quasi-reference counter electrode
RHE	reversible hydrogen electrode
RI	reactive intermediate
SECCM	scanning electrochemical cell microscopy
SECM	scanning electrochemical microscopy
SEM	scanning electron microscopy
SEPM	scanning electrochemical probe microscopy
SERS	surface-enhanced Raman scattering
SICM	scanning ion conductance microscopy
STEM	scanning transmission electron microscopy

REFERENCES

(1) Seh, Z. W.; Kibsgaard, J.; Dickens, C. F.; Chorkendorff, I.; Nørskov, J. K.; Jaramillo, T. F. Combining Theory and Experiment in Electrocatalysis: Insights into Materials Design. *Science* **2017**, *355* (6321), eaad4998.

(2) Bard, A. J. Inner-Sphere Heterogeneous Electrode Reactions. Electrocatalysis and Photocatalysis: The Challenge. *J. Am. Chem. Soc.* **2010**, *132* (22), 7559−7567.

(3) Schmickler, W.; Santos, E. *Interfacial Electrochemistry*, 2nd ed.; Springer: Heidelberg, New York, 2010.

(4) Benck, J. D.; Hellstern, T. R.; Kibsgaard, J.; Chakthranont, P.; Jaramillo, T. F. Catalyzing the Hydrogen Evolution Reaction (HER) with Molybdenum Sulfide Nanomaterials. *ACS Catal.* **2014**, *4* (11), 3957−3971.

(5) Climent, V.; Feliu, J. M. Thirty Years of Platinum Single Crystal Electrochemistry. *J. Solid State Electrochem.* **2011**, *15* (7−8), 1297−1315.

(6) Rodriguez, P.; Koper, M. T. M. Electrocatalysis on Gold. *Phys. Chem. Chem. Phys.* **2014**, *16* (27), 13583−13594.

(7) O'Mullane, A. P. from Single Crystal Surfaces to Single Atoms: Investigating Active Sites in Electrocatalysis. *Nanoscale* **2014**, *6* (8), 4012−4026.

(8) Farias, M. J. S.; Cheuquepan, W.; Camara, G. A.; Feliu, J. M. Disentangling Catalytic Activity at Terrace and Step Sites on Selectively Ru-Modified Well-Ordered Pt Surfaces Probed by CO Electrooxidation. *ACS Catal.* **2016**, *6* (5), 2997−3007.

(9) Seidel, Y. E.; Schneider, A.; Jusys, Z.; Wickman, B.; Kasemo, B.; Behm, R. J. Mesoscopic Mass Transport Effects in Electrocatalytic Processes. *Faraday Discuss.* **2009**, *140* (0), 167−184.

(10) Zou, N.; Zhou, X.; Chen, G.; Andoy, N. M.; Jung, W.; Liu, G.; Chen, P. Cooperative Communication within and between Single Nanocatalysts. *Nat. Chem.* **2018**, *10* (6), 607−614.

(11) Pfisterer, J. H. K.; Liang, Y.; Schneider, O.; Bandarenka, A. S. Direct Instrumental Identification of Catalytically Active Surface Sites. *Nature* **2017**, *549*, 74.

(12) Unwin, P. R.; Güell, A. G.; Zhang, G. Nanoscale Electrochemistry of sp^2 Carbon Materials: From Graphite and Graphene to Carbon Nanotubes. *Acc. Chem. Res.* **2016**, *49* (9), 2041−2048.

(13) Güell, A. G.; Cuharuc, A. S.; Kim, Y.-R.; Zhang, G.; Tan, S.-y.; Ebejer, N.; Unwin, P. R. Redox-Dependent Spatially Resolved Electrochemistry at Graphene and Graphite Step Edges. *ACS Nano* **2015**, *9* (4), 3558−3571.

(14) Bentley, C. L.; Perry, D.; Unwin, P. R. Stability and Placement of Ag/AgCl Quasi-Reference Counter Electrodes in Confined Electrochemical Cells. *Anal. Chem.* **2018**, *90* (12), 7700−7707.

(15) Bentley, C. L.; Kang, M.; Maddar, F. M.; Li, F.; Walker, M.; Zhang, J.; Unwin, P. R. Electrochemical Maps and Movies of the Hydrogen Evolution Reaction on Natural Crystals of Molybdenite (MoS_2): Basal vs. Edge Plane Activity. *Chem. Sci.* **2017**, *8* (9), 6583−6593.

(16) Bentley, C. L.; Kang, M.; Unwin, P. R. Nanoscale Structure Dynamics within Electrocatalytic Materials. *J. Am. Chem. Soc.* **2017**, *139* (46), 16813−16821.

(17) Kang, M.; Perry, D.; Bentley, C. L.; West, G.; Page, A.; Unwin, P. R. Simultaneous Topography and Reaction Flux Mapping at and around Electrocatalytic Nanoparticles. *ACS Nano* **2017**, *11* (9), 9525−9535.

(18) Mariano, R. G.; McKelvey, K.; White, H. S.; Kanan, M. W. Selective Increase in Co_2 Electroreduction Activity at Grain-Boundary Surface Terminations. *Science* **2017**, *358* (6367), 1187−1192.

(19) Alzahrani, H.; Bentley, C.; Burrows, R.; Cao, C.; Cai, Q.; Chikere, C.; Crooks, R. M.; Dunevall, J.; Edwards, M.; Ewing, A.; Gao, R.; Hillman, R.; Kahram, M.; Kanoufi, F.; Kranz, C.; Lemineur, J.-F.; Long, Y.; McKelvey, K.; Mirkin, M.; Moore, S.; Nogala, W.; Ren, H.; Schuhmann, W.; Unwin, P.; Vezzoli, A.; White, H.; Willets, K.; Yang, Z.; Ying, Y. Dynamics of Nanointerfaces: General Discussion. *Faraday Discuss.* **2018**, *210*, 451−479.

(20) Patel, A. N.; Collignon, M. G.; O'Connell, M. A.; Hung, W. O. Y.; McKelvey, K.; Macpherson, J. V.; Unwin, P. R. A New View of Electrochemistry at Highly Oriented Pyrolytic Graphite. *J. Am. Chem. Soc.* **2012**, *134* (49), 20117−20130.

(21) Snowden, M. E.; Güell, A. G.; Lai, S. C. S.; McKelvey, K.; Ebejer, N.; O'Connell, M. A.; Colburn, A. W.; Unwin, P. R. Scanning Electrochemical Cell Microscopy: Theory and Experiment for Quantitative High Resolution Spatially-Resolved Voltammetry and Simultaneous Ion-Conductance Measurements. *Anal. Chem.* **2012**, *84* (5), 2483−2491.

(22) Byers, J. C.; Güell, A. G.; Unwin, P. R. Nanoscale Electrocatalysis: Visualizing Oxygen Reduction at Pristine, Kinked, and Oxidized Sites on Individual Carbon Nanotubes. *J. Am. Chem. Soc.* **2014**, *136* (32), 11252−11255.

(23) Jaramillo, T. F.; Jørgensen, K. P.; Bonde, J.; Nielsen, J. H.; Horch, S.; Chorkendorff, I. Identification of Active Edge Sites for Electrochemical H_2 Evolution from MoS_2 Nanocatalysts. *Science* **2007**, *317* (5834), 100−102.

(24) Aaronson, B. D. B.; Chen, C. H.; Li, H. J.; Koper, M. T. M.; Lai, S. C. S.; Unwin, P. R. Pseudo-Single-Crystal Electrochemistry on Polycrystalline Electrodes: Visualizing Activity at Grains and Grain Boundaries on Platinum for the Fe^{2+}/Fe^{3+} Redox Reaction. *J. Am. Chem. Soc.* **2013**, *135* (10), 3873−3880.

(25) Chen, C.-H.; Meadows, K. E.; Cuharuc, A.; Lai, S. C. S.; Unwin, P. R. High Resolution Mapping of Oxygen Reduction Reaction Kinetics at Polycrystalline Platinum Electrodes. *Phys. Chem. Chem. Phys.* **2014**, *16* (34), 18545−18552.

(26) Bentley, C. L.; Andronescu, C.; Smialkowski, M.; Kang, M.; Tarnev, T.; Marler, B.; Unwin, P. R.; Apfel, U. P.; Schuhmann, W. Local Surface Structure and Composition Control the Hydrogen Evolution Reaction on Iron Nickel Sulfides. *Angew. Chem., Int. Ed.* **2018**, *57* (15), 4093−4097.

(27) Bentley, C. L.; Unwin, P. R. Nanoscale Electrochemical Movies and Synchronous Topographical Mapping of Electrocatalytic Materials. *Faraday Discuss.* **2018**, *210*, 365−379.

(28) Clausmeyer, J.; Masa, J.; Ventosa, E.; Ohl, D.; Schuhmann, W. Nanoelectrodes Reveal the Electrochemistry of Single Nickelhydroxide Nanoparticles. *Chem. Commun.* **2016**, *52* (11), 2408−2411.

(29) Brasiliense, V.; Clausmeyer, J.; Berto, P.; Tessier, G.; Combellas, C.; Schuhmann, W.; Kanoufi, F. Monitoring Cobalt-Oxide Single Particle Electrochemistry with Subdiffraction Accuracy. *Anal. Chem.* **2018**, *90* (12), 7341−7348.

(30) Huang, K.; Clausmeyer, J.; Luo, L.; Jarvis, K.; Crooks, R. M. Shape-Controlled Electrodeposition of Single Pt Nanocrystals onto Carbon Nanoelectrodes. *Faraday Discuss.* **2018**, *210*, 267−280.

(31) Shan, X.; Patel, U.; Wang, S.; Iglesias, R.; Tao, N. Imaging Local Electrochemical Current via Surface Plasmon Resonance. *Science* **2010**, *327* (5971), 1363−1366.

(32) Shan, X.; Diez-Perez, I.; Wang, L.; Wiktor, P.; Gu, Y.; Zhang, L.; Wang, W.; Lu, J.; Wang, S.; Gong, Q.; Li, J.; Tao, N. Imaging the Electrocatalytic Activity of Single Nanoparticles. *Nat. Nanotechnol.* **2012**, *7* (10), 668−672.

(33) Jiang, D.; Jiang, Y.; Li, Z.; Liu, T.; Wo, X.; Fang, Y.; Tao, N.; Wang, W.; Chen, H.-Y. Optical Imaging of Phase Transition and Li-Ion Diffusion Kinetics of Single $LiCoO_2$ Nanoparticles During Electrochemical Cycling. *J. Am. Chem. Soc.* **2017**, *139* (1), 186−192.

DOI: 10.1021/jacs.8b09828
J. Am. Chem. Soc. 2019, 141, 2179−2193

(34) Huang, B.; Bates, M.; Zhuang, X. W. Super-Resolution Fluorescence Microscopy. *Annu. Rev. Biochem.* **2009**, *78*, 993−1016.
(35) Hao, R.; Fan, Y.; Howard, M. D.; Vaughan, J. C.; Zhang, B. Imaging Nanobubble Nucleation and Hydrogen Spillover during Electrocatalytic Water Splitting. *Proc. Natl. Acad. Sci. U. S. A.* **2018**, *115* (23), 5878−5883.
(36) Hussein, H. E. M.; Maurer, R. J.; Amari, H.; Peters, J. J. P.; Meng, L.; Beanland, R.; Newton, M. E.; Macpherson, J. V. Tracking Metal Electrodeposition Dynamics from Nucleation and Growth of a Single Atom to a Crystalline Nanoparticle. *ACS Nano* **2018**, *12* (7), 7388−7396.
(37) Ustarroz, J.; Hammons, J. A.; Altantzis, T.; Hubin, A.; Bals, S.; Terryn, H. A Generalized Electrochemical Aggregative Growth Mechanism. *J. Am. Chem. Soc.* **2013**, *135* (31), 11550−11561.
(38) Ustarroz, J.; Ornelas, I. M.; Zhang, G.; Perry, D.; Kang, M.; Bentley, C. L.; Walker, M.; Unwin, P. R. Mobility and Poisoning of Mass-Selected Platinum Nanoclusters during the Oxygen Reduction Reaction. *ACS Catal.* **2018**, *8* (8), 6775−6790.
(39) Peng, Y.-Y.; Qian, R.-C.; Hafez, M. E.; Long, Y.-T. Stochastic Collision Nanoelectrochemistry: A Review of Recent Developments. *ChemElectroChem* **2017**, *4* (5), 977−985.
(40) Quinn, B. M.; Van 't Hof, P. G.; Lemay, S. G. Time-Resolved Electrochemical Detection of Discrete Adsorption Events. *J. Am. Chem. Soc.* **2004**, *126* (27), 8360−1.
(41) Xiao, X. Y.; Bard, A. J. Observing Single Nanoparticle Collisions at an Ultramicroelectrode by Electrocatalytic Amplification. *J. Am. Chem. Soc.* **2007**, *129* (31), 9610−9612.
(42) Zhou, Y.-G.; Rees, N. V.; Compton, R. G. The Electrochemical Detection and Characterization of Silver Nanoparticles in Aqueous Solution. *Angew. Chem., Int. Ed.* **2011**, *50* (18), 4219−4221.
(43) Robinson, D. A.; Edwards, M. A.; Ren, H.; White, H. S. Effects of Instrumental Filters on Electrochemical Measurement of Single-Nanoparticle Collision Dynamics. *ChemElectroChem* **2018**, *5* (20), 3059−3067.
(44) Kang, M.; Perry, D.; Kim, Y.-R.; Colburn, A. W.; Lazenby, R. A.; Unwin, P. R. Time-Resolved Detection and Analysis of Single Nanoparticle Electrocatalytic Impacts. *J. Am. Chem. Soc.* **2015**, *137* (34), 10902−10905.
(45) Bentley, C. L.; Kang, M.; Unwin, P. R. Time-Resolved Detection of Surface Oxide Formation at Individual Gold Nanoparticles: Role in Electrocatalysis and New Approach for Sizing by Electrochemical Impacts. *J. Am. Chem. Soc.* **2016**, *138* (39), 12755−12758.
(46) Ustarroz, J.; Kang, M.; Bullions, E.; Unwin, P. R. Impact and Oxidation of Single Silver Nanoparticles at Electrode Surfaces: One Shot Versus Multiple Events. *Chem. Sci.* **2017**, *8* (3), 1841−1853.
(47) Oja, S. M.; Robinson, D. A.; Vitti, N. J.; Edwards, M. A.; Liu, Y.; White, H. S.; Zhang, B. Observation of Multipeak Collision Behavior during the Electro-Oxidation of Single Ag Nanoparticles. *J. Am. Chem. Soc.* **2017**, *139* (2), 708−718.
(48) Ma, W.; Ma, H.; Chen, J.-F.; Peng, Y.-Y.; Yang, Z.-Y.; Wang, H.-F.; Ying, Y.-L.; Tian, H.; Long, Y.-T. Tracking Motion Trajectories of Individual Nanoparticles Using Time-Resolved Current Traces. *Chem. Sci.* **2017**, *8* (3), 1854−1861.
(49) Robinson, D. A.; Liu, Y.; Edwards, M. A.; Vitti, N. J.; Oja, S. M.; Zhang, B.; White, H. S. Collision Dynamics during the Electrooxidation of Individual Silver Nanoparticles. *J. Am. Chem. Soc.* **2017**, *139* (46), 16923−16931.
(50) Kleijn, S. E. F.; Lai, S. C. S.; Miller, T. S.; Yanson, A. I.; Koper, M. T. M.; Unwin, P. R. Landing and Catalytic Characterization of Individual Nanoparticles on Electrode Surfaces. *J. Am. Chem. Soc.* **2012**, *134* (45), 18558−18561.
(51) Brasiliense, V.; Patel, A. N.; Martinez-Marrades, A.; Shi, J.; Chen, Y.; Combellas, C.; Tessier, G.; Kanoufi, F. Correlated Electrochemical and Optical Detection Reveals the Chemical Reactivity of Individual Silver Nanoparticles. *J. Am. Chem. Soc.* **2016**, *138* (10), 3478−3483.
(52) Hao, R.; Fan, Y.; Zhang, B. Imaging Dynamic Collision and Oxidation of Single Silver Nanoparticles at the Electrode/Solution Interface. *J. Am. Chem. Soc.* **2017**, *139* (35), 12274−12282.
(53) Edwards, M. A.; German, S. R.; Dick, J. E.; Bard, A. J.; White, H. S. High-Speed Multipass Coulter Counter with Ultrahigh Resolution. *ACS Nano* **2015**, *9* (12), 12274−12282.
(54) Yu, Y.; Sundaresan, V.; Bandyopadhyay, S.; Zhang, Y.; Edwards, M. A.; McKelvey, K.; White, H. S.; Willets, K. A. Three-Dimensional Super-resolution Imaging of Single Nanoparticles Delivered by Pipettes. *ACS Nano* **2017**, *11* (10), 10529−10538.
(55) Kai, T.; Zoski, C. G.; Bard, A. J. Scanning Electrochemical Microscopy at the Nanometer Level. *Chem. Commun.* **2018**, *54* (16), 1934−1947.
(56) Momotenko, D.; McKelvey, K.; Kang, M.; Meloni, G. N.; Unwin, P. R. Simultaneous Interfacial Reactivity and Topography Mapping with Scanning Ion Conductance Microscopy. *Anal. Chem.* **2016**, *88* (5), 2838−2846.
(57) Sa, N.; Lan, W.-J.; Shi, W.; Baker, L. A. Rectification of Ion Current in Nanopipettes by External Substrates. *ACS Nano* **2013**, *7* (12), 11272−11282.
(58) Page, A.; Perry, D.; Young, P.; Mitchell, D.; Frenguelli, B. G.; Unwin, P. R. Fast Nanoscale Surface Charge Mapping with Pulsed-Potential Scanning Ion Conductance Microscopy. *Anal. Chem.* **2016**, *88* (22), 10854−10859.
(59) Momotenko, D.; Byers, J. C.; McKelvey, K.; Kang, M.; Unwin, P. R. High-Speed Electrochemical Imaging. *ACS Nano* **2015**, *9* (9), 8942−8952.
(60) Weber, M. L.; Wilson, A. J.; Willets, K. A. Characterizing the Spatial Dependence of Redox Chemistry on Plasmonic Nanoparticle Electrodes Using Correlated Super-Resolution Surface-Enhanced Raman Scattering Imaging and Electron Microscopy. *J. Phys. Chem. C* **2015**, *119* (32), 18591−18601.
(61) Zhang, Y.; Lucas, J. M.; Song, P.; Beberwyck, B.; Fu, Q.; Xu, W.; Alivisatos, A. P. Superresolution Fluorescence Mapping of Single-Nanoparticle Catalysts Reveals Spatiotemporal Variations in Surface Reactivity. *Proc. Natl. Acad. Sci. U. S. A.* **2015**, *112* (29), 8959−8964.
(62) Sambur, J. B.; Chen, T. Y.; Choudhary, E.; Chen, G. Q.; Nissen, E. J.; Thomas, E. M.; Zou, N. M.; Chen, P. Sub-Particle Reaction and Photocurrent Mapping to Optimize Catalyst-Modified Photoanodes. *Nature* **2016**, *530* (7588), 77−80.

DOI: 10.1021/jacs.8b09828
J. Am. Chem. Soc. 2019, 141, 2179−2193